Computational Materials Science 148 (2018) 216–223

Contents lists available at ScienceDirect

Computational Materials Science

journal homepage: www.elsevier.com/locate/commatsci

Effect of the nanopore on ferroelectric domain structures and switching properties

He Zhao [a], Pingping Wu [a,*], Lifei Du [b,*], Huiling Du [b]

[a] Department of Materials Science and Engineering, Xiamen Institute of Technology, Xiamen, Fujian 361021, China
[b] College of Materials Science and Engineering, Xi'an University of Science and Technology, Xi'an, Shaanxi 710054, China

ARTICLE INFO

Article history:
Received 19 December 2017
Received in revised form 7 February 2018
Accepted 7 February 2018

Keywords:
Nanopore
Domain structure
Switching properties
Ferroelectrics
Phase field model

ABSTRACT

Porous ferroelectrics have some special properties and features for specific promising applications. The nanopores structure have been observed in experiments may have great influence on the ferroelectric domain structures and the switching properties of ferroelectrics. In this study, we proposed a phase field model to predict the domain structures of porous ferroelectrics and their evolution under a switching electric field. The effects of the pores size/shape on domain structure, switching properties, and dielectric/piezoelectric properties are investigated and analyzed. The simulated hysteresis loop is in good agreement with experimental reports. It is shown that the porosity can strongly affect the ferroelectric domain size, and furthermore, will influence the hysteresis loop. Therefore controlling the porosity of ferroelectrics may provide a possible way to adjust the properties of porous ferroelectric materials.

1. Introduction

Porous ferroelectric materials can be tailored to achieve special properties and features for specific applications [1,2]. By controlling ferroelectric porosity with its size/shape/orientation/intercon nectivity shows enhanced properties including piezoelectric coefficient [3–8], dielectric constant [5–8], and ferroelectric properties [7–9]. Porous ferroelectrics also show higher pyroelectric harvesting for its potential energy harvesting applications [10–12]. These properties enhancement suggest that porous ferroelectrics have great potential in various applications.

Very recently, nanosized pores formed in nano-thin film or nanowires also have attracted great attentions. Ferreira et al. reported nanoporous piezo- and ferroelectric thin films from sol-gel solutions [13], and noticed ferroelectric properties are enhanced in nanoporous films [14]. Kalinin et al. studied local ferroelectric properties and switching polarization using piezoresponse force spectroscopy and have revealed an enhanced piezoresponse from the nanostructured films [15]. Nanopores with a typical diameter of around 10 nm are discovered in ferroelectric nanowires, nanopores didn't break the monocrystallinity and the negative pressure results in enhancement of tetragonality, Curie temperature, spontaneous polarization and piezoelectric [16]. Please note that nanoporous ferroelectrics/piezoelectrics are highly promising as platforms to construct mechanical/magnetoelectric composites with a designed architecture.

Many experimentalists would like to avoid pores to fetch a perfect crystal. However, the generation of porosity in ferroelectrics can be seen as an avenue to achieve lighter materials with enhanced or optimized ferroelectric properties. Thus, it is important to study the roles played by pores for improving/adjusting ferroelectric properties. Many theoretical works have been developed to expect the properties, e.g., a finite element model (FEM) built by Mitoseriu et al. investigated permittivity and tenability for isotropic/elongated pores in 2D [17] and 3D interconnectivity [18,19]. The switching properties also have been investigated by the multiscale nonlinear finite element simulation [20] or 3D Ginzburg-Landau theory based finite element model [21], and the simulated ferroelectric properties can be compared to experimental observations. The switching properties of Nb-PZT (Lead Zirconate Titanate) ceramics with anisotropic porosity (~40% relative porosity) were investigated by comparison with the dense ceramics (~5% relative porosity) of the same composition by means of the first-order reversal curve analysis [22]. Khachaturyan et al. used FEM simulations of the statistical field-distributions to study switching process of the ferroelectric ceramics with pores of different size, shape, and orientation. Simulation results predicted the roles played by the shape isometric/anisometric, size, distribution of the pores in ferroelectric switching process [23]. Some very early works done by Li et al. [24] and Brown et al. [25] with a finite element model show that the remanent polarization decreases with

---

* Corresponding authors.
E-mail addresses: pingpingwu@xit.edu.cn (P. Wu), dulifei@xust.edu.cn (L. Du).

https://doi.org/10.1016/j.commatsci.2018.02.022
0927-0256/

the increase of porosity density. The effect of the shape and displacement was also analyzed in three dimensional [25].

However, above studies didn't include any ferroelectric domain structures, which is strongly affiliated with the ferroelectric properties, and also, domain structure affiliated switching process is less investigated. A significant differences in remanent polarization (P_r) between porous and dense PZT films was observed by Trolier-McKinstry et al. [26], which suggests that the porosity has an impact on domain wall motion and may further contribute to the switching properties [27,28]. Weng et al. used a thermodynamic model to simulate the hysteresis loop of ferroelectric crystal on various porosity [29].

Recently, phase field method have great potential in simulating porous ceramics [30], ferroelectric domain structures [31] and various types of magnetoelectric materials [32–35]. The switching properties also have been simulated using this method [35–38]. In this paper, we would like to solve the following problems: (i) what is the domain structure like when a specific shaped pore (isometric/anisometric) is introduced into the ferroelectrics, (ii) what is the hysteresis loop and the remanent polarization (P_r)/coercive electric field (E_c) like with this porous material. (iii) The relationship between the hysteresis loop and the domain structures, how the pores influence on the switching properties and the P_r/E_c. In this work, the ferroelectric domain structure of $BaTiO_3$ with various shapes/sizes of pores was studied by employing the phase-field dynamical model with solving the time dependent Ginzburg-Landau (TDGL) equations. The switching properties of $BaTiO_3$ with nanopores are also illustrated with its domain structure evolution, and the influence of the porosity on the ferroelectric domains and switching properties have been studied.

2. Phase field model with pores

Consider four types of energy to describe the domain of ferroelectric in phase-field model, where the total free energy of ferroelectric materials includes bulk free energy, domain wall energy, electrostatic energy and elastic deformation energy, i.e.,

$$F_{electric} = F_{land} + F_{wall} + F_{elec} + F_{elas}, \tag{1}$$

where F_{land} can be expressed by an eight-order Landau polynomial:

$$\begin{aligned} F_{land}(P_i) = \int_V & \alpha_1(P_1^2+P_2^2+P_3^2) + \alpha_{11}(P_1^4+P_2^4+P_3^4) \\ & + \alpha_{12}(P_1^2P_2^2+P_2^2P_3^2+P_1^2P_3^2) + \alpha_{111}(P_1^6+P_2^6+P_3^6) \\ & + \alpha_{112}[P_1^2(P_2^4+P_3^4)+P_2^2(P_1^4+P_3^4)+P_3^2(P_1^4+P_2^4)] \\ & + \alpha_{123}P_1^1P_2^2P_3^3 + \alpha_{1111}(P_1^8+P_2^8+P_3^8) + \alpha_{1112}[P_1^6(P_2^2+P_3^2) \\ & + P_2^6(P_1^2+P_3^2) + P_3^6(P_1^2+P_2^2)] + \alpha_{1122}(P_1^4P_2^4+P_2^4P_3^4+P_1^4P_3^4) \\ & + \alpha_{1123}(P_1^4P_2^2P_3^2+P_2^4P_1^2P_3^2+P_3^4P_2^2P_2^2)d^3x, \end{aligned} \tag{2}$$

where a_1, a_{ij}, a_{ijk}, and a_{ijkl} are the phenomenological Landau expression coefficients, P_i (i = 1, 2, 3) is the spontaneous polarization which set as the order parameters, thus the ferroelectric domain structure can be described by the spatial distribution of P_i. V is the volume of the simulated system and $d^3x = dx_1dx_2dx_3$.

The ferroelectric domain wall energy is given by:

$$F_{wall}(\partial P_i/\partial x_j) = \int_V \left[\frac{1}{2}G_{ijkl}\frac{\partial P_i}{\partial x_j}\frac{\partial P_k}{\partial x_l}\right]d^3x, \tag{3}$$

where G_{ijkl} is coefficient of gradient energy and $G_{ijkl} = G_{klij}$.

The electrostatic energy can be written as:

$$F_{elec}(P_i, E_i) = -\int_V \left(\frac{1}{2}\varepsilon_b\varepsilon_0E_i^2 + E_iP_i\right)d^3x, \tag{4}$$

where E_i represents electric field component, which depends on the polarization distribution and the boundary conditions, ε_0 is the vacuum permittivity, and ε_b is the background relative dielectric permittivity.

According to Khachaturyan's elastic theory [39], the elastic energy F_{elas} can be written as:

$$F_{elas}(P_i, \varepsilon_{ij}) = \int_V \left[\frac{1}{2}c_{ijkl}(\varepsilon_{ij} - Q_{ijkl}P_kP_l)(\varepsilon_{kl} - Q_{klij}P_iP_j)\right]d^3x, \tag{5}$$

where ε_{ij} is strain and c_{ijkl} is the elastic stiffness tensor. Q_{ijkl} is the electrostrictive coefficient.

In the current work, we introduce a static phase field $\eta(r)$ to distinguish the ferroelectric phase and the pores phase, as the phase field η do not evolve with time, the position and the size of the pores are fixed. If $\eta(r) = 1$, position r is occupied by the ferroelectric phase, whereas for $\eta(r) = 0$ means position r is occupied by the pore phase. The total free-energy of a ferroelectric material with pores includes the contribution of ferroelectric energy and pore energy, i.e.

$$F_{total} = \eta(r)\cdot F_{electric} + (1-\eta(r))F_{pores}, \tag{6}$$

for simplicity, we set $F_{pores} = 0$, which means the pore phase has no contribution to the total energy of the materials, especially for predicting the domain structures of ferroelectrics.

With all the energetic contributions, the temporal and spatial evolution of the polarization distribution of ferroelectrics can be described by the Time-Dependent Ginzburg-Landau (TDLG) equations,

$$\frac{\partial P_i(r,t)}{\partial t} = -L\frac{\delta F_{total}}{\delta P_i(r,t)}, \quad (i = 1,2,3) \tag{7}$$

where t is time, and L is kinetic coefficient.

All the corresponding coefficients are employed here: $\alpha_1 = 4.124(T\text{-}388) \times 10^5$, $\alpha_{11} = -2.097 \times 10^8$, $\alpha_{12} = 7.974 \times 10^8$, $\alpha_{111} = 1.294 \times 10^9$, $\alpha_{112} = -1.905 \times 10^9$, $\alpha_{123} = 2.500 \times 10^9$, $\alpha_{1111} = 3.863 \times 10^{10}$, $\alpha_{1112} = 2.529 \times 10^{10}$, $\alpha_{1122} = 1.637 \times 10^{10}$, $\alpha_{1123} = 1.367 \times 10^{10}$, $c_{11} = 1.78 \times 10^{11}$, $c_{12} = 0.964 \times 10^{11}$, $c_{44} = 1.22 \times 10^{11}$, $Q_{11} = 0.10$, $Q_{12} = -0.034$, $Q_{44} = 0.029$, where c_{ij} and Q_{ij} are the Voigt notation for c_{ijkl} and Q_{ijkl}. All the coefficients are in SI unit and T in Kelvin [40].

3. Simulation results

We systematic studied the effects of various shapes/sizes of pores on the domain structure and switching properties. Firstly, we illustrated the simulation of ferroelectric switching process by a hysteresis loop with the evolution of ferroelectric domain structure. Then we assumed the shape of the pores are ideal perfect isometric geography, e.g. square shaped or circle shaped pores. After that, the situation of the anisometric shaped pores were considered, like using a rectangle/ellipse shaped pores with various aspect ratio. Finally we discussed the ferroelectric/dielectric/piezoelectric properties by comparing the P_r, rectangularity factor, dielectric constant and piezoelectric constant with experimental results.

3.1. Hysteresis loop with domain structure for porous $BaTiO_3$

Fig. 1(a, b) illustrates a complete Polarization-Electric field hysteresis loop (PE loop) with the domain evolution of $BaTiO_3$ crystal with a squared shaped single pore under a switching field along the x direction. The simulation size is 256 nm × 256 nm with the pore size of 96 nm × 96 nm. The domain structures A-I in Fig. 1b are corresponding to the points A-I in Fig. 1a, respectively. The microstructure evolution under the

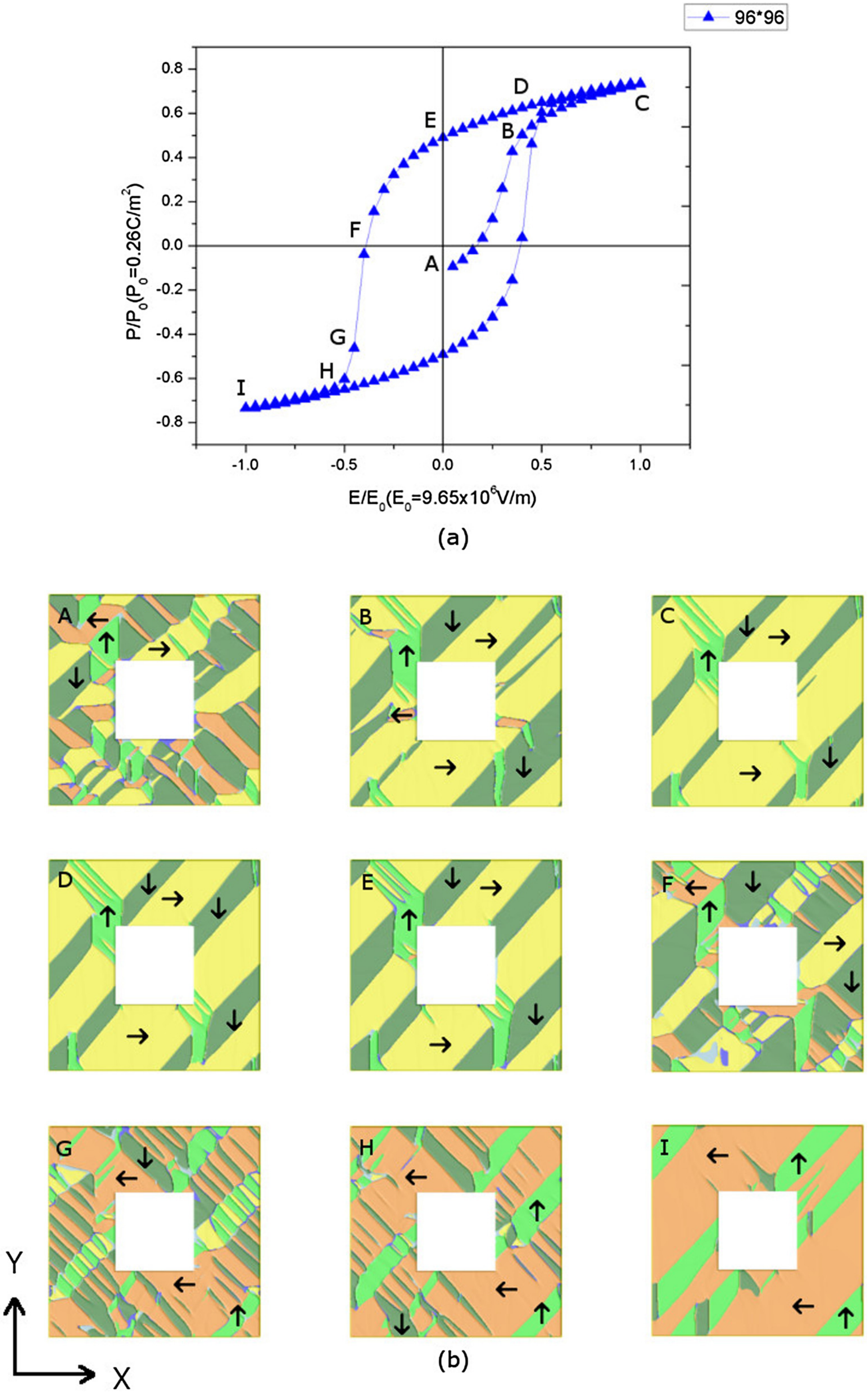

Fig. 1. (a) A typical switching loop of $BaTiO_3$ with a square shaped pore, (b) the domain structure evolution during the switching process, domain structure A-I are corresponding to the point A-I of (a).

electric field occurs through two mechanisms, the domain wall movement and the polarization rotation. At point A, as no electric field applied, four tetragonal domains with their directions along $+x/-x/+y/-y$ are observed in this 2D simulations. With the increase of the external field, the x domains are favored by the electric field, in the first stage of the initial polarization, the $-x$ domains and partial y domains shrink and disappear, lead to a jump in the switching loop. The comparison between the domain structures of B and C show that, minor changes are observed in the domain structures and the total polarization climbs very slowly. We found that the polarization rotation mechanisms governed this process. It is important to note that the switching processes didn't end up in a single domain state since the grain structures or defects are not considered in our current simulation. During the depolarization stage, the domain structure didn't change, the polarization rotation makes the 90 degree domain wall movement and the volume fraction increase of *y* domains. However, at the remanent polarization point E, a small new domain with opposite polarization ($-x$ domain) is observed at the pore surface. If the external applied field increased along $-x$ direction, one can see the $-x$ domains nucleate and grow (see point F). Meanwhile, in order to decrease the electrostatic energy, one can see $+y$ domains appear in the $+x$ domains. In the following stage, a narrow stripe structure formed at point G lead to the whole structure switched with a rapid decrease in the PE loops. Finally, the structure is switched to $-x/-y$ domain structure, which is separated by 90 degree domain walls at $-x$ electric field max (point I), previous $+x$ domains shrink and is replaced by $+y$ domain, while the $-y$ domains expands and switched to $-$x direction.

3.2. Squared/circle shaped pores

To study the effect of pore sizes on the domain structures and switching properties, Fig. 2 shows simulated ferroelectric domain structures with various squared shaped (b–d) and circle shaped (e–g) pores absence of applied field. Fig. 2a shows a perfect ferroelectric domain structure of $BaTiO_3$. One can see the classical stair-shaped domain structure which is in consistent with previous experimental works; *x* domains and *y* domains are separated by 90 degrees domain walls. To investigate the effect of the pores, we embedded a square shaped pore at the center of the domain structure and increased its size from 32 × 32 nm to 160 × 160 nm. If increase the size of the pores, the ferroelectric domains can be changed to a complex structure, with a number of small domains and domain walls. The presence of domain walls involve other energy cost, especially for 90 degrees domain walls, which will generate inhomogeneities in the strain field. For a small pore size of 32 × 32 (nm^2), the introducing of pores changes the domain structures. The symmetry of domain structure is broken and lead to a complicated pattern. On the surface of the pore, small domains of closure with triangular cross-sections appears, as predicted in theory and experiments [41]. It should be noticed that this small closure domain structure is mostly driven by the reduction of electrostatic energy. The polarization direction of the ferroelectric domain was expected to along the pores surface to avoid the charge accumulation and lower the electrostatic energy. The simulation results are similar to Zhang's work on the ferroelectric domain structures with triangle anti-dot array [42], in which the polarization is perpendicular to the edge and lead to the splitting of the ferroelectric domain. By increasing the size of pores (Fig. 2(c,d)), the number of triangular shaped closure increases and lead to a reduction of the average size of domains by introducing more domain walls. In such a case, branching–pattern domains are observed at the pore interfaces, resulting in the formation of triangular cross-section patterns. This structure contains a large density of domain walls, but most importantly, it is the results of the balancing the domain wall energy and electrostatic energy to minimize the total free energy.

In experiments, Circle/Spherical shaped pores are more natural. As shown in Fig. 2(e), for an almost dense ferroelectric with a small pore (diameter = 64 nm), minor topological change is observed in domain structures. A small $-y$ domain grow from the pores interface in the parent $+y$ domain, which separates the domain into two segments with two 180 degree domain wall. It is seen that domains maintain the stair-shaped structure and exhibit centro-symmetry. A very small triangular shaped $-x$ domain can be seen at the intersection point of pore boundary/$+y$ domain/$-y$ domain. Fig. 2(f, g) show the domain structures obtained with large pores (diameter = 128/160 nm). The domain

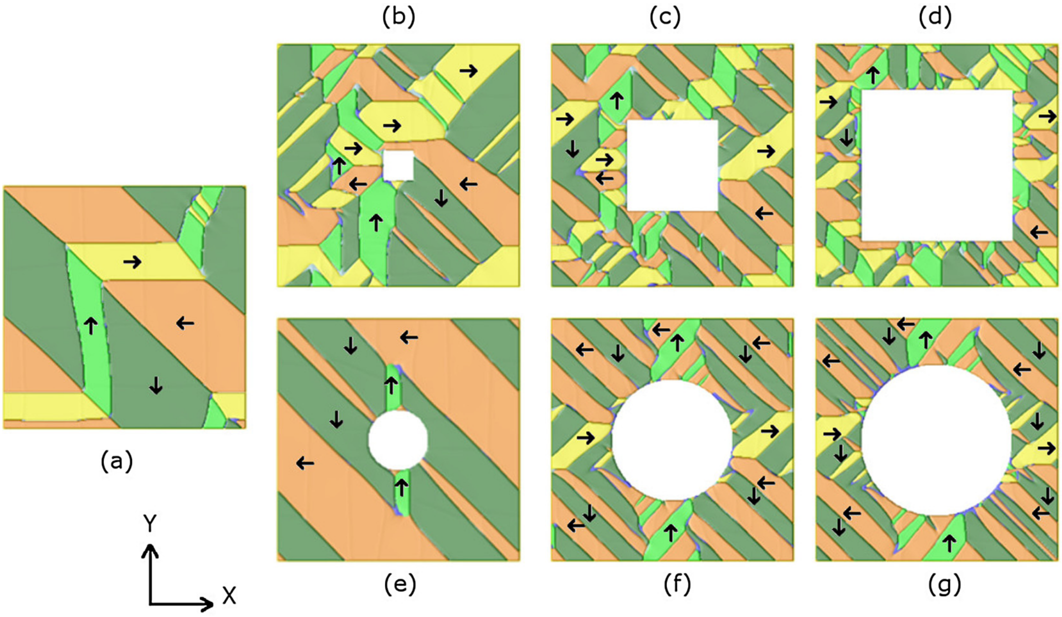

Fig. 2. (a) Stair shaped ferroelectric domain structure with no pores. The domains colored yellow, orange, light green, dark green represents polarization vector along the +x, −x, +y, −y axis, respectively; (b–d) Domain structures with square shaped pores of various sizes of (b) 32 × 32 (c) 96 × 96 (d) 160 × 160 (unit:nm^2); (e–g) domain structures with circle shaped pores of various diameters of (e) D = 64 nm (f) D = 128 nm (g) D = 160 nm.

structure become quite different and are strongly affected by the increase of the pores' diameter. For example, the element of a twinned domains composed of $-x/-y$ domain is replaced by the one composed of $+x/-y$ domain along the x direction, in contract, a twinned domains composed of $-x/-y$ domain is replaced by the one composed of $-x/-y$ structure along the y direction, and the size of the domain decreases if the pores' diameter raised. This phenomenon may be due to the depolarization field for minimizing the electrostatic energy. If the pore size is small, especially, smaller than the domain size, it's easy to predict that the effect of pores on domain structure is limited. When the size of pores is large enough, the domains with its polarization along all the possible directions appear, as the polarizations is favored to be parallel to the pore/ceramic boundaries.

For a complete study of pores size effect on the switching properties, the hysteresis loops of ferroelectrics (P-E loop) was computed for square shaped pores (Fig. 3(a)) and circle shaped pores (Fig. 3(b)), at different size levels. These simulations show indeed that the pore size strongly influences the hysteresis loop. Comparing to perfect ferroelectric, introducing a small pore in the structure will lead to a very small increase in E_c for both shaped pores. After that, both the remanent polarization and the coercive field decrease continuously with increasing of pore sizes. The decrease can be easily understood because that the volume fraction of ferroelectrics is reduced when considering large sized pores. Large pore size also lowered the rectangularity of the loops. The evolution of domain structures during the switching process are similar to Fig. 1. Further details about the dielectric and piezoelectric properties will be discussed in the following section.

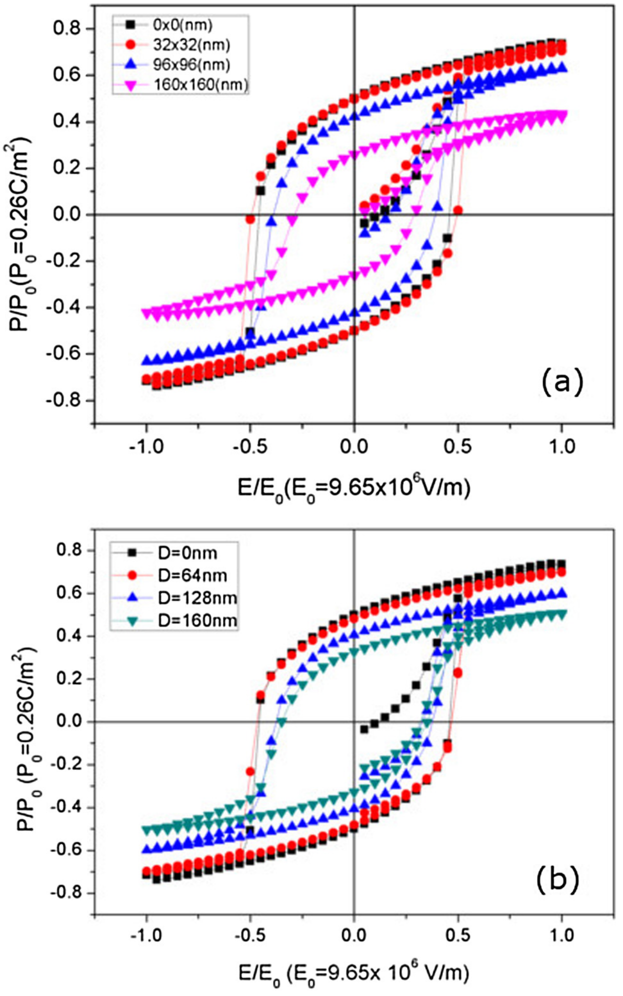

Fig. 3. P-E hysteresis loops of ferroelectrics with (a) square shaped pores (b) circle shaped pores.

3.3. Rectangle/ellipse shaped pores

Comparing to ideal isometric shaped pores, anisometric shaped pores are more realistic. By controlling the shape of pores, one can engineer the switching properties of ferroelectrics to satisfy practical applications. One possible way to create anisometric shaped pores is to elongate the pores through applying external mechanical stress. In our current work, simulations were taken using rectangle/ellipse shaped pores with various aspect ratio but similar porosity level (~25%) to investigate the effect of anisometric shaped pores on domain structure and switching properties. Fig. 4 (a–d) shows domain structures with rectangle shaped pores of aspect ratio varies from 1:1.5 to 3:1. Interestingly, comparing to the domain structure of square shaped pores, the symmetry broken of the pores makes the ferroelectric domain structure simpler. The distribution of polarization vector also formed a stairs shaped centro-symmetric structure. It is important to note that periodical boundary condition is employed in this current simulation, small pieces domains are found near the short edge of the rectangle shaped pores, which can be explained by the depolarization field caused by the boundary effect. Small twinned fragmental domains can introduce more domain wall energy but lower the cost of electrostatic energy, and lead to total free energy minimum. Specifically, when the aspect ratio raises, the balancing between the proportion of *x* domains and *y* domains is broken, in the sequence of (a-b), the *y* domain stripes gets broader than the *x* domain stripes, which indicated that the *y* domains are favored by high aspect ratio pores. Meanwhile similar process is seen in the sequence of (c-d), in which the *x* domains expand and *y* domains shrink.

Fig. 4(e–h) show the domain structures with ellipse shaped pores for semi major/minor axis of 2:1/3:1, placing along *y* axis (as shown in Fig. 4e, f) or *x* axis (as shown in Fig. 4g, h). A very simple twinned domain pattern is obtained when ellipse shaped pores were implanted. Some needle-like/triangle shaped domains are found near the pores boundary in order to lower the total free energy. We noted that the ellipse shaped pores like to stay in the domains whose polarization direction along the semi major axis of the pores, this domain picture is self-organized in the absence of the applied field, and energetically preferable. This result may suggest a possible way to engineering ferroelectric domains through controlling the pores shape.

Comparing all the P-E loops of elongated shaped pores, as all of these domain structures have similar pores fraction, only minor differences are observed in the switching loops, as shown in Fig. 5. For the structures with pores having the long axis parallel to the external field, a small increase of ramenent polarization is seen, but the coercive field is less influenced by the shapes and elongated directions of pores.

3.4. Ferroelectric, dielectric and piezoelectric properties

For ferroelectric/piezoelectric applicability reasons, it is important to understand the relationship between the pores of ceramics and its ferroelectric, dielectric and piezoelectric properties. The simulated properties for porous $BaTiO_3$ ferroelectrics, including remanent polarization (P_r), coercive field (E_c), rectangularity factor (P_r/P_s), dielectric constant (ε_{33}) and piezoelectric

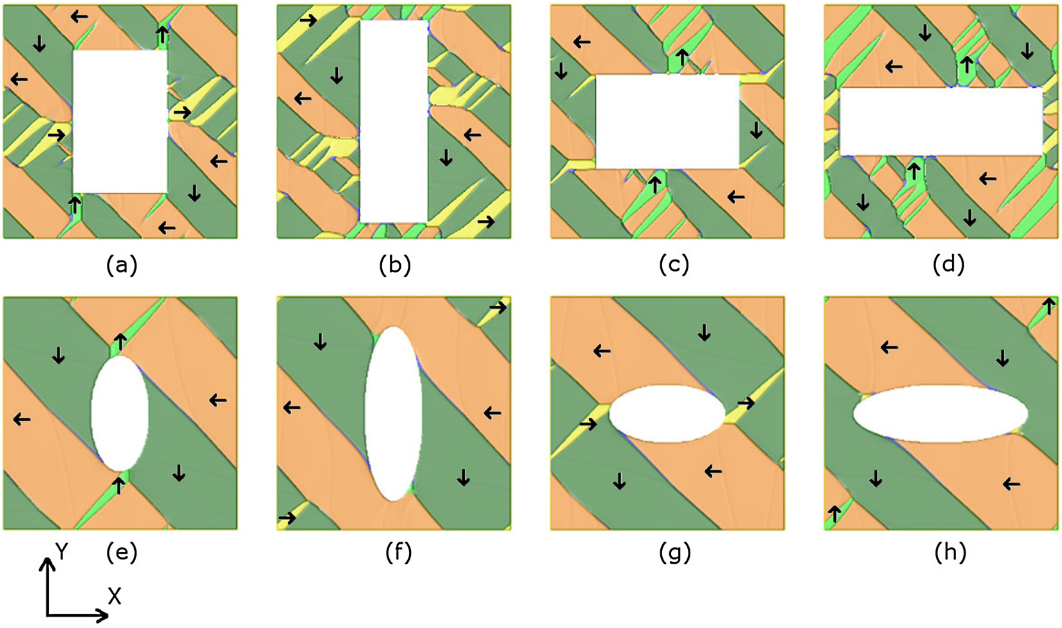

Fig. 4. (a-d) The domain structures with rectangle shaped pores of various aspect ratio (a)1:1.5 (b)1:3 (c)1.5:1 (d)3:1, respectively; (e-h) The domain structures with ellipse shaped pores, the major radius/minor radius is chosen to be 2:1 or 3:1 placing along the y axis (e, f) or x axis (g, h).

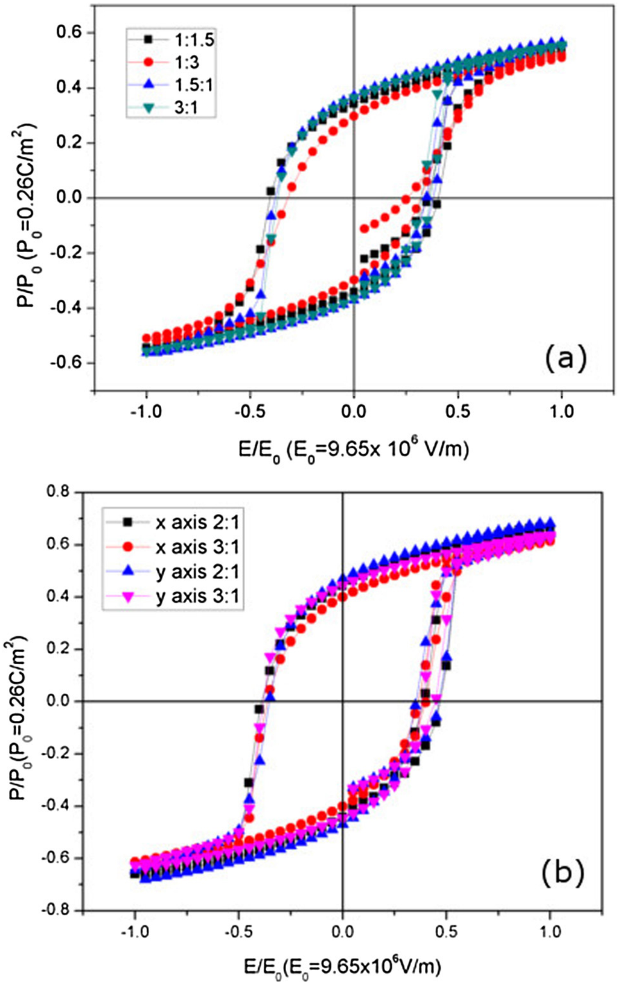

Fig. 5. P-E hysteresis loops of ferroelectrics with (a) rectangle shaped pores (b) ellipse shaped pores.

coefficient (d_{33}) are shown in Table 1. Different from thermodynamic calculations, for a multi-domain system in phase field model, the dielectric constant is estimated by taking the slope of the polarization at maximum applied electric field to the origin ($\varepsilon_{33} = \varepsilon_{11} = (\Delta\overline{P}_1)/\Delta E_1 = \overline{P}|_{max}/E_{max}$), the piezoelectric constant also can be calculated in the similar way of $d_{33} = d_{11} = (\Delta\bar{e}_1)/\Delta E_1 = \bar{e}|_{max}/E_{max} = Q_{11} \times P_1^2 + Q_{12} \times (P_2^2 + P_3^2)/E_{max}$, where $\bar{e}_1$ is the average value of strain along the *x* direction. The remanent polarization, rectangularity factor, dielectric constant and piezoelectric coefficient versus porosity for porous ceramics are comparatively presented in Fig. 6 (a–d). The result show that the Ferroelectric/Dielectric/Piezoelectric Properties are clearly influence by the porosity of the $BaTiO_3$ ceramic as well as the nanopore shape.

For ferroelectric properties, a strong decrease of the P_r is observed for high porous ferroelectrics. It is essential to note that for a given porosity, higher remanent polarization and rectangularity factor is found in circle shaped porous ferroelectric, and the coercive field is less affected by the geometrical configuration. A maximum value of rectangularity factor (~0.73) is found in an ellipse shaped porous ceramics, with the ellipse its semi major/minor axis of 2:1, placing along *x* axis. Rectangle shaped pores with aspect ratio of 1:3 exhibited lowest rectangularity factor of 0.58. These simulated results indicated that the rectangularity factor can be influenced by the anisometric geometrical configuration of the pores. The dielectric constant and piezoelectric coefficient continuously reduces when increasing the porosity level: ε_{33} varies from 2240 for dense ceramics to 1317 for 39% porosity, and d_{33} varies from 371pC/N for dense ceramics to 129pC/N for 39% porosity. The effect of the porosity is dominant while shape of the pores have minor contribution to ε_{33} and d_{33}. Enhanced dielectric/piezoelectric properties are also observed for elongated pores with the major axis oriented parallel to the applied field direction. These simulated value ($P_r/\varepsilon_{33}/d_{33}$) can be compared with experimental results. According to these calculations, porous ceramics with well-controlled porosity/pores shape may provide enhanced ferroelec tric/dielectric/piezoelectric properties.

Table 1
Ferroelectric, Dielectric and Piezoelectric properties of porous structure in this work. $P_0 = 0.26 C/m^2$ and $E_0 = 9.65 \times 10^6 V/m$.

Shape	Porosity	P_r/P_0	E_c/E_0	P_r/P_s	ε_{33}	d_{33} (P_c/N)
Square 0 × 0	0	0.50054	0.45	0.699	2240	371
Square 32 × 32	1.56%	0.49853	0.5	0.705	2223	368
Square 96 × 96	14.06%	0.42198	0.4	0.668	1920	275
Square 160 × 160	39.06%	0.26012	0.3	0.618	1317	130
Circle d = 64	4.91%	0.48204	0.45	0.690	2137	341
Circle d = 128	19.63%	0.40676	0.35	0.678	1815	244
Circle d = 160	30.68%	0.32754	0.35	0.650	1545	177
Rectangle 1:1.5	24.76%	0.34154	0.45	0.628	1619	189
Rectangle 1:3	25.06%	0.29762	0.35	0.583	1583	184
Rectangle 1.5:1	24.76%	0.3712	0.4	0.661	1718	222
Rectangle 3:1	25.06%	0.36551	0.4	0.656	1676	210
Ellipse 2:1 at y axis	9.82%	0.44233	0.4	0.671	2029	311
Ellipse 3:1 at y axis	14.73%	0.4009	0.4	0.653	1892	270
Ellipse 2:1 at x axis	9.82%	0.46969	0.4	0.731	2076	326
Ellipse 3:1 at x axis	14.73%	0.44511	0.4	0.709	1938	281

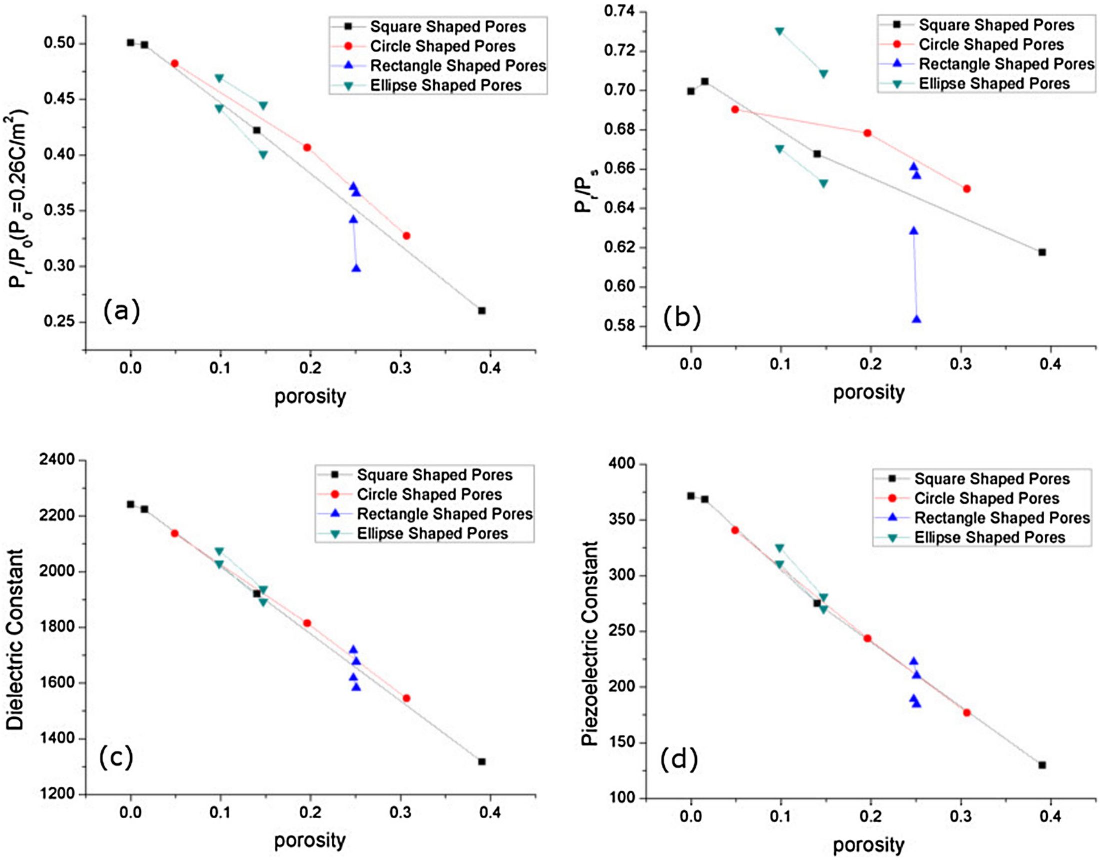

Fig. 6. The remanent polarization (a), rectangularity factor (b), dielectric constant (c) and piezoelectric coefficient (d) versus porosity calculated for various shaped porous ceramics at different porosity levels.

4. Conclusion

In summary, porous $BaTiO_3$ ceramics were simulated using a phase field model based on Gingzburg Landau theory and Khachaturyan's elastic theory. The present work reports domain structures, switching hysteresis loops and dielectric/piezoelectric features in various porous ferroelectrics with different pores shape/size. We found that (1) increasing the porosity of ceramics reduces the remanent polarization, dielectric constant and piezoelectric constant, (2) the rectangularity factor is strongly influenced by the geometrical configuration of the pores. A maximum value around 0.73 is observed in ceramics with ellipse shaped pores while ceramics with rectangle shaped pores exhibited a minimum value of 0.58, (3) ferroelectric domains can be engineered through implanting specific shaped pores. The ferroelectric /dielectric /piezoelectric properties have been calculated for the porous ferroelectrics that correlate well with experimental results. It is suggested that the possibility of the optimized properties can be designed or adjusted through controlling the porosity or pores shape of the ferroelectrics for its potential applications.

Acknowledgement

The author P. P. W. gratefully acknowledge the support of Science and Technology Program of Fujian Educational Committee under Grant No. JA14370 and outstanding young research talents program (2016) in colleges and universities of Fujian province.

The author L. Du gratefully acknowledge the support of the National Natural Science Foundation of China (grant numbers 51501146, 51372197), the Cultivating Research Program of Xi'an University of Science and Technology (grant number 201701), and the Key Innovation Team of Shaanxi Province (grant number 2014KCT-04).

References

[1] U.T.G. André, R. Studart, E. Tervoort, L.J. Gauckler, J. Am. Ceram. Soc. 89 (2006) 1771.
[2] C. Galassi, J. Eur. Ceram. Soc. 26 (2006) 2951–2958.
[3] M.A.E. Koray Akdogan, Ahmad Safari, IEEE Trans. Ultrason. Ferroelect. Freq. Control 52 (2005) 746.
[4] T. Xu, C.-A. Wang, Mater. Des. 91 (2016) 242–247.
[5] W. Liu, J. Xu, R. Lv, Y. Wang, H. Xu, J. Yang, Ceram. Int. 40 (2014) 2005–2010.
[6] R. Guo, C.-A. Wang, A. Yang, J. Eur. Ceram. Soc. 31 (2011) 605–609.
[7] H. Zhang, J. Li, B. Zhang, Acta Materialia 55 (2007) 171–181.
[8] T. Zeng, X. Dong, C. Mao, Z. Zhou, H. Yang, J. Eur. Ceram. Soc. 27 (2007) 2025–2029.
[9] V. Annapu Reddy, N.P. Pathak, R. Nath, Curr. Appl. Phys. 12 (2012) 451–455.
[10] Y. Zhang, Y. Bao, D. Zhang, C.R. Bowen, L. Pilon, J. Am. Ceram. Soc. 98 (2015) 2980–2983.
[11] J. Roscow, Y. Zhang, J. Taylor, C.R. Bowen, Eur. Phys. J. Special Topics 224 (2015) 2949–2966.
[12] J.I. Roscow, J. Taylor, C.R. Bowen, Ferroelectrics 498 (2016) 40–46.
[13] P. Ferreira, R.Z. Hou, A. Wu, M.G. Willinger, P.M. Vilarinho, J. Mosa, C. Laberty-Robert, C. Boissiere, D. Grosso, C. Sanchez, Langmuir: the ACS journal of surfaces and colloids 28 (2012) 2944–2949.
[14] A. Castro, P. Ferreira, B.J. Rodriguez, P.M. Vilarinho, J. Mater. Chem. C 3 (2015) 1035–1043.
[15] M.A. McLachlan, D.W. McComb, M.P. Ryan, A.N. Morozovska, E.A. Eliseev, E.A. Payzant, S. Jesse, K. Seal, A.P. Baddorf, S.V. Kalinin, Adv. Funct. Mater. 21 (2011) 941–947.
[16] A. Kvasov, L.J. McGilly, J. Wang, Z. Shi, C.S. Sandu, T. Sluka, A.K. Tagantsev, N. Setter, Nat. Commun. 7 (2016) 12136.
[17] L. Padurariu, L. Curecheriu, C. Galassi, L. Mitoseriu, Appl. Phys. Lett. 100 (2012) 252905.
[18] C. Padurariu, L. Padurariu, L. Curecheriu, C. Ciomaga, N. Horchidan, C. Galassi, L. Mitoseriu, Ceram. Int. 43 (2017) 5767–5773.
[19] R. Stanculescu, C.E. Ciomaga, L. Padurariu, P. Galizia, N. Horchidan, C. Capiani, C. Galassi, L. Mitoseriu, J. Alloy. Compd. 643 (2015) 79–87.
[20] Y. Uetsuji, T. Hata, T. Oka, H. Kuramae, K. Tsuchiya, Comput. Mater. Sci. 106 (2015) 100–110.
[21] F. Gheorghiu, L. Padurariu, M. Airimioaei, L. Curecheriu, C. Ciomaga, C. Padurariu, C. Galassi, L. Mitoseriu, J. Am. Ceram. Soc. 100 (2017) 647–658.
[22] L. Stoleriu, A. Stancu, L. Mitoseriu, D. Piazza, C. Galassi, Phys. Rev. B 74 (2006).
[23] R. Khachaturyan, S. Zhukov, J. Schultheiß, C. Galassi, C. Reimuth, J. Koruza, H. von Seggern, Y.A. Genenko, J. Phys. D Appl. Phys. 50 (2017) 045303.
[24] Z. Li, C. Wang, C. Chen, Comput. Mater. Sci. 27 (2003) 381–392.
[25] M.A. Brown, J.L. Ding, J.R. Robbins, Ferroelectr. Lett. Sect. 34 (2007) 1–21.
[26] R.L. Johnson-Wilke, R.H. Wilke, M. Wallace, A. Rajashekhar, G. Esteves, Z. Merritt, J.L. Jones, S. Trolier-McKinstry, IEEE Trans. Ultrason. Ferroelect. Freq. Control 62 (2015) 46–55.
[27] F. Xu, S. Trolier-McKinstry, W. Ren, B. Xu, Z.L. Xie, K.J. Hemker, J. Appl. Phys. 89 (2001) 1336–1348.
[28] R.J. Zednik, A. Varatharajan, M. Oliver, N. Valanoor, P.C. McIntyre, Adv. Funct. Mater. 21 (2011) 3104–3110.
[29] W.F. Li, G.J. Weng, Acta Materialia 52 (2004) 2489–2496.
[30] L. Du, P. Zhang, L. Wang, B. Zheng, H. Du, Comput. Mater. Sci. 131 (2017) 196–201.
[31] L.-Q. Chen, J. Am. Ceram. Soc. 91 (2008) 1835–1844.
[32] J.-M. Hu, C.-G. Duan, C.-W. Nan, L.-Q. Chen, NPJ Computat. Mater. 3 (2017).
[33] F. Xue, L. Liang, Y. Gu, I. Takeuchi, S.V. Kalinin, L.-Q. Chen, Appl. Phys. Lett. 106 (2015) 012903.
[34] P.P. Wu, X.Q. Ma, J.X. Zhang, L.Q. Chen, Phil. Mag. 90 (2010) 125–140.
[35] G. Cao, Y. Cao, H. Huang, L.-Q. Chen, X. Ma, Comput. Mater. Sci. 115 (2016) 208–213.
[36] P. Wu, X. Ma, Y. Li, V. Gopalan, L.-Q. Chen, Appl. Phys. Lett. 100 (2012) 092905.
[37] P. Wu, X. Ma, Y. Li, C.-B. Eom, D.G. Schlom, V. Gopalan, L.-Q. Chen, Appl. Phys. Lett. 107 (2015) 122906.
[38] S. Pan, Q. Li, Q. Liu, Comput. Mater. Sci. 140 (2017) 244–252.
[39] A.G. Khachaturyan, Theory of structural transformations in solids, Dover Publications, 2008.
[40] Y.L. Li, L.E. Cross, L.Q. Chen, J. Appl. Phys. 98 (2005) 064101.
[41] L.D. Landau, E.M. Lifshits, Electrodynamics of Continuous Media, 2nd edition., Butterworth-Heinemann, 1984.
[42] Y. Zhang, Y.L. Wang, P. Chu, Y.L. Xie, Z.B. Yan, J.M. Liu, Comput. Mater. Sci. 108 (2015) 301–308.